Geophys. J. Int. (2003) **153,** 175–186

Detection of layer boundaries in wells using multi-electrode resistivity data

A. Weller,[1] M. Furche[1] and J. H. Schön[2]

[1]*Institut für Geophysik, Technische Universität Clausthal, Arnold-Sommerfeld-Str.* 1, D-38678 *Clausthal-Zellerfeld, Germany. E-mail: andreas.weller@tu-clausthal.de*

[2]*Joanneum Research, Institut für Angewandte Geophysik, Roseggerstr.* 17, A-8700 *Leoben, Austria*

Accepted 2002 October 22. Received 2002 September 12; in original form 2002 February 28

SUMMARY

Multi-electrode resistivity data can be used to compute the measurable response for conventional and focused configurations. Some of them are appropriate for detecting layer boundaries. Three different configurations are investigated concerning their suitability for identification of bed boundaries: a second difference configuration, a combined lateral configuration and a Laterolog-7. A normalized apparent resistivity is used as an indication parameter for detection of horizontal bed boundaries for the first two configurations. For the Laterolog-7, the curve of the logarithm of the quotient of the two current ratios is used. The boundaries are indicated by extreme values in the relevant curves. The ability of layer identification of the three configurations is tested with synthetic and measured data.

The parameter curves provide different information: the peaks indicate the presence of a layer boundary, the sign of the peak (positive or negative) indicates the type of transition (resistive–conductive or conductive–resistive). The Laterolog-7 shows the best results concerning resolution and accuracy. It yields additional information as the absolute values are related to the resistivity contrast of the adjacent beds. The combined lateral configuration also proved to be suitable for detection of layer boundaries. The second difference configuration only indicates the transition from conductive to resistive layers. It is severely affected by noisy data.

Key words: borehole geophysics, electrical resistivity, layer boundaries, numerical techniques.

1 INTRODUCTION

The continuous measurement of apparent resistivity along a well yields a resistivity log that when correctly interpreted can furnish valuable geological information. Electrical logging methods were first developed and applied in order to identify layers and distinguish hydrocarbon-bearing from water-saturated zones. Today the electrical methods are an important part of saturation studies of all logging programs. The specific environmental conditions of an electrode array in the mud, the influence of the invaded zone and the limited thickness of the layers promoted different tools with particular radial and vertical characteristics.

Compared with the conventional single-configuration probes multi-electrode resistivity tools provide a larger number of data in a single run and will replace the older tools. The wide range of electrode spacings guarantees different radii of investigation. The greater data density acquired by multi-electrode tools results in improved axial and radial resolution of the borehole environment. A generalized sketch of a vertical borehole in a layered medium is shown in Fig. 1. A borehole with a radius r_0 is filled with mud of resistivity ρ_{m}. A sequence of layers with different thickness h_{n} and formation resistivity $\rho_{t,n}$ is regarded. If the mud fluid penetrates in a permeable rock formation an invaded zone is formed. The radius $r_{i,n}$ and the resistivity $\rho_{i,n}$ of the invaded zone depend on mud pressure, formation permeability and the salinity of mud and the formation water. The measured apparent resistivity is influenced by all the parameters given in Fig. 1. Log interpretation aims to determine these parameters from the available logs.

Different multi-electrode tools have been presented over the past 20 years. Schön & Weller (1984) designed a tool with one current electrode and four potential electrodes. Using reciprocity and the principle of superposition, the four normal logs are combined to generate the response of a Laterolog with seven equally spaced electrodes. Pusch *et al.* (1988) increase the number of potential electrodes to 20. The voltage readings of this tool can be combined to synthesize 13 types of Laterolog-7 with different electrode spacings. It should be mentioned that the same principle has also been used to approximate a Laterolog-7 from a single normal log (Pusch 1990; Whitman *et al.* 1990).

Yuratich & Meger (1984) describe a *resistivity profile tool* consisting of 12 voltage monitoring electrodes. Vallinga *et al.* (1991) use this tool to test the synthetic focusing concept. It was demonstrated

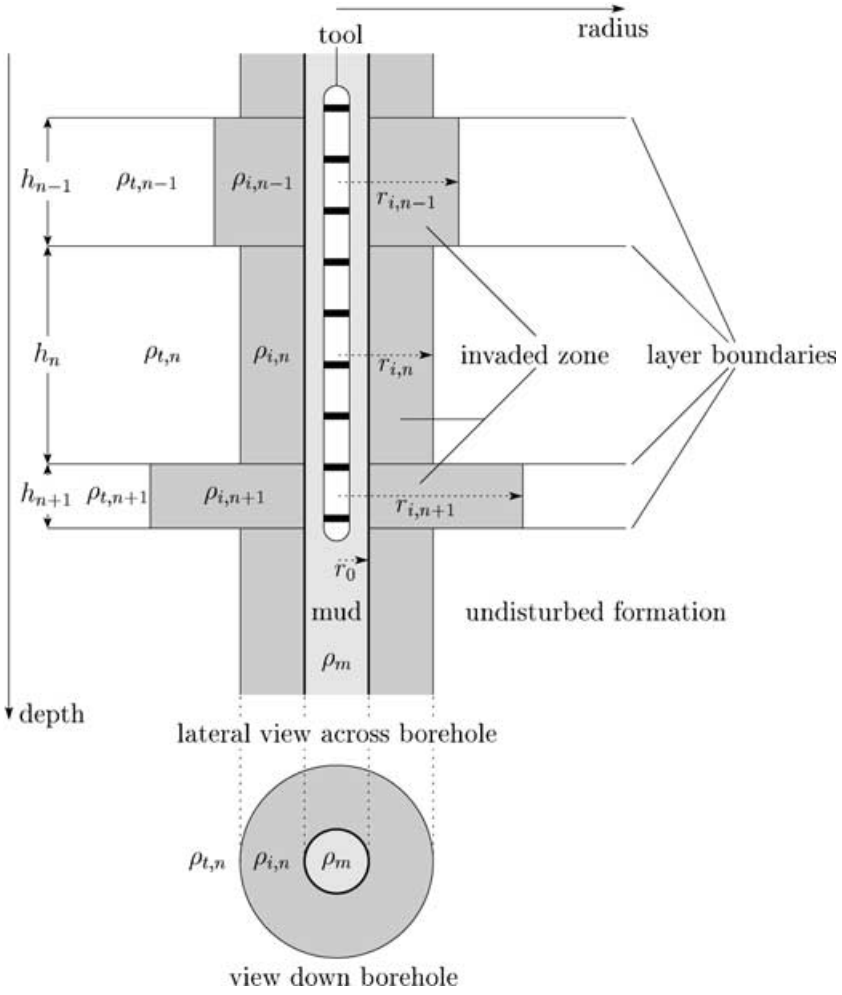

Figure 1. Scheme of the geometric situation and the distribution of resistivities in the environment of a well.

that a good vertical resolution can be achieved without any technical focusing. Hakvoort *et al.* (1998) and Zhang & Zhou (2002) present the results of data inversion with a *high-definition lateral log*. The tool consists of a single current electrode and 18 potential measurement electrodes. It records eight voltages and 16 first differences. The voltage or normal readings are based on a pole–pole configuration with a current injection electrode A and only one potential electrode M in the borehole. The return electrodes are placed at large distances. A first difference corresponds to the lateral reading that is based on a pole–dipole configuration that measures the potential gradient along the borehole axis.

Sophisticated inversion algorithms perform the transformation of the measured data into a reliable resistivity model (Whitman *et al.* 1989; Hakvoort *et al.* 1998; Fan 1998; Zhang & Zhou 2002). Since any resistivity data set is incomplete and affected by noise the inversion is from the mathematical point of view an ill-posed problem. A solution can only be found if additional constraints are applied. In a certain class of models the model is chosen as a solution that yields the best fit to the measured data. Even in a given class of models the data do not guarantee a unique solution. The principle of equivalence is also valid in resistivity logging. Only by enlarging the database or by using *a priori* information can the ambiguity be remarkably reduced. Mezzatesta & Eckard (1995) propose a joint inversion method based on the data of both galvanic and induction tools to improve the accuracy of the model parameters. If the positions of layer boundaries are known the number of free model parameters is reduced. Consequently, the reliability of the inversion results is improved. Zhang *et al.* (2002) present an algorithm to derive the layer boundaries from gamma-ray, density, neutron porosity and resistivity logs.

In this paper we show that the positions of layer boundaries can be extracted from multi-electrode resistivity data. Conventional configurations such as normal or lateral curves give only a rough estimate of the position of layer boundaries. However, special electrode configurations are able to identify layer boundaries with better resolution and accuracy. The response of these configurations can be generated from multi-electrode data. The tool considered in our investigation consists of nine equally spaced electrodes. It records eight voltages at each depth. All other quantities are calculated by algebraic operations using the principles of superposition and reciprocity. Three different synthetic configurations are investigated: a second difference configuration, a combined lateral configuration and a Laterolog-7. The ability of these configurations to resolve bed boundaries is tested with synthetic and measured data.

2 DETECTION PARAMETERS OF SYNTHETIC CONFIGURATIONS

Fig. 2(a) shows a schematic of the design of the nine-electrode resistivity tool used, which provides the data used for the investigation.

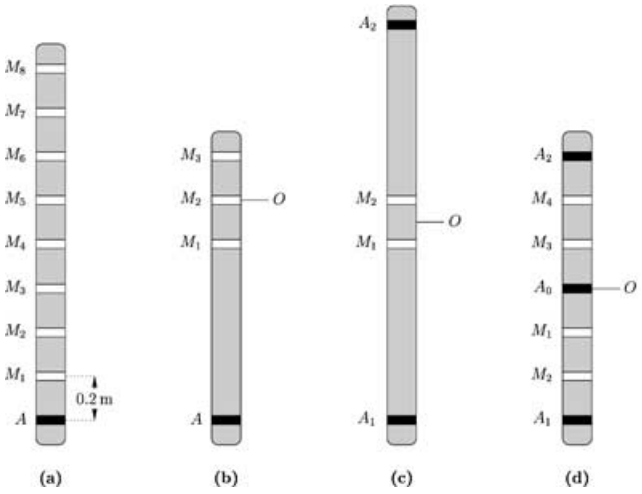

Figure 2. Scheme of the electrode arrangement of the: (a) nine-electrode resistivity tool, (b) second difference configuration, (c) combined lateral configuration and (d) Laterolog-7.

The current injection electrode is denoted by A, the eight potential electrodes are denoted by M_1–M_8. The return electrodes B and N are located far outside the borehole. The distance between two neighbouring electrodes is 0.2 m. The tool records eight normal logs.

The theoretical background of all calculations is given by the potential of a pole–pole configuration in a homogeneous space

$$V(A, M) = \rho_{\text{hom}} \frac{I}{4\pi \overline{AM}}, \tag{1}$$

which presents the potential measured at an electrode M if a current I is injected at electrode A. $\overline{AM}$ is the distance between the pair of electrodes and ρ_{hom} is the constant resistivity. The measured potential differences of all configurations are calculated using a superposition of the individual potentials.

2.1 Second difference configuration

A schematic of the second difference configuration is shown in Fig. 2(b). Hakvoort *et al.* (1998) use configurations of this type to determine layer boundaries. The current electrode A is located near the lower end of the tool. The three potential electrodes (M_1–M_3) are arranged at the upper part of the tool. For this special configuration, the distances are $\overline{AM_1} = 0.8$ m, $\overline{AM_2} = 1.0$ m and $\overline{AM_3} = 1.2$ m. The reference level of the tool coincides with the position of electrode M_2 and is denoted by O. The apparent resistivity is defined as

$$\rho_{\text{a}} = \frac{k}{I}[V(A, M_1) - 2V(A, M_2) + V(A, M_3)], \tag{2}$$

where

$$k = \frac{4\pi}{1/\overline{AM_1} - 2/\overline{AM_2} + 1/\overline{AM_3}} \tag{3}$$

is the configuration factor. The potential values used in eq. (2) are provided by the readings at the electrodes M_4, M_5 and M_6 of the nine-electrode resistivity tool in Fig. 2(a). To obtain an indication parameter for detecting layer boundaries that is independent of the general resistivity level, the apparent resistivity ρ_{a} is related to the mud resistivity ρ_{m}.

2.2 Combined lateral configuration

The second configuration is a combination of two lateral configurations. Simple lateral configurations are only sensitive to a single type of layer boundary with respect to the change in resistivity. For example, the lower boundary of a resistive layer in a conductive environment is indicated as a strong maximum value in the log by a configuration with the electrode A near the upper end of the tool. The position of the upper boundary is only indicated by a small minimum. If the electrode A is located at the lower end of the tool the upper boundary is accentuated by a maximum of apparent resistivity. Fig. 2(c) shows the symmetric combination of two lateral configurations, which is able to identify the upper and the lower boundary of any layer. Near the ends of the tool are the current injection electrodes A_1 and A_2 that have the same polarity. The two potential electrodes M_1 and M_2 are located symmetrically about the centre of the tool, which is identical to the reference point O. The electrode distances of the chosen configuration are $\overline{A_1M_1} = \overline{A_2M_2} = 0.8$ m and $\overline{A_1M_2} = \overline{A_2M_1} = 1.0$ m. This configuration represents the superposition of two single lateral configurations. The potential differences resulting from both current electrodes, which inject the same current strength, are added. The apparent resistivity of such a configuration is calculated using the following equation:

$$\rho_{\text{a}} = \frac{k}{I}[V(A_1, M_1) - V(A_1, M_2) + V(A_2, M_1) - V(A_2, M_2)]. \tag{4}$$

The response of this tool can be assembled from the readings of the nine-electrode tool. The voltages $V(A_1, M_1)$ and $V(A_1, M_2)$ are extracted from the readings at electrodes M_4 and M_5 of the nine-electrode resistivity tool with A_1 at the original position of A. To obtain the readings $V(A_2, M_1)$ the nine-electrode tool has to be moved four steps upward. In this position, the principle of reciprocity

$$V(M_1, A_2) = V(A_2, M_1) \tag{5}$$

is applied. The determination of the potential $V(A_2, M_2)$ requires an additional step upward. In this position the reading $V(A, M_4)$ of the nine-electrode tool yields the required potential.

Since the potentials cancel each other out in a homogeneous formation this tool represents a *zero-potential* configuration. The resulting configuration factor becomes infinite. However, in the case of an inhomogeneous resistivity distribution (e.g. near a bed boundary), there exists a non-vanishing (positive or negative) potential difference. Since rather than the absolute value of apparent resistivity, it is the general behaviour of the curve that is of interest, an arbitrary factor can be chosen to scale the curve. We selected the factor

$$k = \frac{2\pi}{1/\overline{A_1M_1} - 1/\overline{A_1M_2}}, \tag{6}$$

which considers the geometry of the electrodes. The location of the extreme values of a parameter curve that relates the resulting values of eq. (4) to mud resistivity is considered as an indication parameter for layer boundaries.

2.3 Laterolog-7

Fig. 2(d) shows the design of a focused resistivity tool consisting of seven electrodes that are equally spaced. The two outer injection electrodes A_1 and A_2, which are called guard electrodes, have the same polarity as the central electrode A_0 that injects a current I_0. The focusing or bucking currents are chosen in such a way that the

potential differences between the two pairs of potential electrodes M_1 and M_2 or M_3 and M_4 vanish, i.e.

$$V(M_1) - V(M_2) = V(M_3) - V(M_4) = 0. \tag{7}$$

This condition is necessary to impede a flow of current parallel to the tool through the borehole mud. Consequently, the current will be focused into the formation. To obey the control conditions (7) a current $I_1 = n_1 I_0$ is injected at electrode A_1 and a current $I_2 = n_2 I_0$ is injected at electrode A_2. The factors n_1 and n_2 are called current ratios. The mid-point between the potential electrodes M_1 and M_2 is regarded as the reference point for the display of the curve of the current ratio n_1. The mid-point between M_3 and M_4 is the reference point of the current ratio n_2 (Pusch 1990). The local extreme values of the current ratios correspond to the actual layer boundaries. In order to obtain only one parameter the quotient of the two current ratio curves is calculated for all depth points. Since the size of the quotient, such as that of the resistivities, varies over several decades, a logarithmic presentation is proposed. The resulting expression $\log(n_1/n_2)$ yields a suitable indication parameter for layer boundaries.

This type of Laterolog-7 can be generated synthetically by combining the readings at electrodes M_1, M_2, M_4 and M_5 of the nine-electrode resistivity tool (Weller 1986).

3 EXAMPLES OF SYNTHETIC DATA

Synthetic data generated for various layered formations are used to demonstrate the ability of different configurations to detect layer boundaries. The synthetic data sets are computed by a numerical forward modelling based on a finite-difference (FD) code (Weller *et al.* 1984; Weller 1986). First, a description of the main features of the finite-difference algorithm is given. Later in this section, the results of forward modelling and boundary detection for three different models—a resistive layer, an invaded layer and a sequence of seven layers—will be presented.

3.1 Finite-difference forward modelling

The aim of forward modelling in geoelectrical investigations is to calculate the apparent resistivity of several electrode configurations for a given conductivity structure $\sigma(\mathbf{r})$. The electric potential V in a non-uniform isotropic medium is governed by the following differential equation:

$$\nabla \cdot [\sigma(\mathbf{r}) \nabla V(\mathbf{r})] = -q(\mathbf{r}), \tag{8}$$

where $q(\mathbf{r})$ is the current source function. It is suitable for transforming eq. (8) into cylindrical coordinates to model the environment of a vertical borehole in a horizontally layered medium. Assuming that the problem is independent of the azimuth angle φ, the potential V and the conductivity σ become a function of just the radius $r = \sqrt{x^2 + y^2}$ and the vertical z-coordinate. Eq. (8) can be rewritten as

$$\frac{\partial}{\partial r}\left[\sigma(r,z)\frac{\partial V(r,z)}{\partial r}\right] + \frac{\partial}{\partial z}\left[\sigma(r,z)\frac{\partial V(r,z)}{\partial z}\right] + \frac{1}{r}\sigma(r,z)\frac{\partial V(r,z)}{\partial r} = -q(r,z). \tag{9}$$

The solution of this differential equation has to satisfy a Neumann boundary condition at the borehole axis

$$\left.\frac{\partial V(r,z)}{\partial r}\right|_{r=0} = 0, \tag{10}$$

and the potential has to vanish at large distances from the current source:

$$\lim_{r,|z|\to\infty} V(r,z) = 0. \tag{11}$$

Since there is no general analytical solution of eqs (9)–(11) numerical methods have to be used. We chose the finite-difference method, which has proved to be an effective tool in direct current and induced polarization modelling (e.g. Mufti 1976; Dey & Morrison 1979; Spitzer 1995; Weller *et al.* 1996) to solve the partial differential eq. (9). The medium is discretized using a 2-D rectangular grid. The basic cells with constant conductivity $\sigma_{i,j}$ are hollow cylinders. Its cross-section is a rectangle with the gridpoint $P_{i,j}$ at the top left-hand corner and side lengths of Δz_i and Δr_j. After integrating eq. (9) over an elemental volume surrounding the central node $P_{i,j}$ and approximating the partial derivatives in the resulting surface integral by a central-difference formula, we obtain for each internal node an equation in the form

$$G_e(i,j)V_{i,j+1} + G_s(i,j)V_{i+1,j} + G_w(i,j)V_{i,j-1} + G_{\mathrm{n}}(i,j)V_{i-1,j} - G_p(i,j)V_{i,j} + I_{i,j} = 0 \tag{12}$$

with the coupling coefficients

$$G_e(i,j) = \pi\left(\frac{r_j}{\Delta r_j} + \frac{1}{2}\right)(\Delta z_{i-1}\sigma_{i-1,j} + \Delta z_i \sigma_{i,j}), \tag{13}$$

$$G_s(i,j) = \pi\left(\frac{r_j}{\Delta z_i}\right)(\Delta r_{j-1}\sigma_{i,j-1} + \Delta r_j \sigma_{i,j}), \tag{14}$$

$$G_w(i,j) = \pi\left(\frac{r_j}{\Delta r_{j-1}} + \frac{1}{2}\right)(\Delta z_{i-1}\sigma_{i-1,j-1} + \Delta z_i \sigma_{i-1,j}), \tag{15}$$

$$G_{\mathrm{n}}(i,j) = \pi\left(\frac{r_j}{\Delta z_{i-1}}\right)(\Delta r_{j-1}\sigma_{i-1,j-1} + \Delta r_j \sigma_{i-1,j}). \tag{16}$$

The Neumann boundary condition in eq. (10) is met if all coupling coefficients G_w at the axis $r = 0$ are vanishing. To meet the requirement of eq. (11) we chose the mixed boundary condition as proposed by Dey & Morrison (1979),

$$\frac{\partial V}{\partial n} + \frac{V}{s}\cos\beta = 0, \tag{17}$$

where s denotes the length of the vector $\mathbf{s}$ connecting the source location and the node at the boundary and β is defined as the angle between $\mathbf{s}$ and the outward normal $\mathbf{n}$ at the boundary plane. The mixed boundary condition considers the asymptotic behaviour of the potential field in a homogeneous medium.

To improve the accuracy around the source position we use the so-called singularity removal proposed by Lowry *et al.* (1989). This procedure is based on a separation of the conductivity model into normal and anomalous parts:

$$\sigma = \sigma_{\mathrm{n}} + \sigma_{\mathrm{a}}, \tag{18}$$

and the potential into normal and anomalous fields:

$$V = V_{\mathrm{n}} + V_{\mathrm{a}}. \tag{19}$$

For these separations, eq. (8) is written as

$$\nabla \cdot \{[\sigma_{\mathrm{n}}(\mathbf{r}) + \sigma_{\mathrm{a}}(\mathbf{r})]\nabla[V_{\mathrm{n}}(\mathbf{r}) + V_{\mathrm{a}}(\mathbf{r})]\} = -q(\mathbf{r}). \tag{20}$$

The normal field V_{n} can easily be calculated for a homogeneous space with constant conductivity σ_{n}:

$$\nabla \cdot [\sigma_{\mathrm{n}}(\mathbf{r}) \nabla V_{\mathrm{n}}(\mathbf{r})] = -q(\mathbf{r}). \tag{21}$$

The subtraction of eq. (21) from eq. (20) results in

$$\nabla \cdot \{[\sigma_{\mathrm{n}}(\mathbf{r}) + \sigma_{\mathrm{a}}(\mathbf{r})]\nabla V_{\mathrm{a}}(\mathbf{r})\} = b(\mathbf{r}) \tag{22}$$

with

$$b(\mathbf{r}) = -\nabla \cdot [\sigma_a(\mathbf{r})\nabla V_n(\mathbf{r})]. \quad (23)$$

Eq. (22) is used instead of eq. (8). The source term $q(\mathbf{r})$ on the right-hand side of eq. (8) is replaced by $b(\mathbf{r})$, which can be calculated directly from the known normal potential distribution V_n and the anomalous part of the conductivity σ_a. The left-hand side has kept its structure. Only the total potential field V is replaced by its anomalous part V_a. Using the separation into normal and anomalous potential fields, the FD approximation is reduced to the computation of the anomalous field. The two parts of the field are added after the FD calculation.

For all internal and boundary nodes a linear equation in the form of eq. (12) is obtained. The set of FD equations is assembled in matrix form

$$\mathbf{Gv} = \mathbf{b}, \quad (24)$$

where $\mathbf{G}$ is called the conductance matrix (Weller *et al.* 1996). The vector $\mathbf{v}$ consists of the unknown potentials V_a at all nodes and the vector $\mathbf{b}$ is calculated according to eq. (23) for all nodes. The conductance matrix is real, symmetric and positive-definite.
The system of algebraic equations with these properties is solved by the conjugate-gradient method (Dey & Morrison 1979; Spitzer 1995; Zhang *et al.* 1995). In order to improve the convergence of the iterative method the conductance matrix is pre-conditioned by the incomplete Cholesky decomposition (Meijerink & van der Vorst 1977).

Our basic grid for forward modelling consists of 21 nodes in the radial direction and 411 nodes in the axial direction. In the radial direction, the node distances increase with radius. In the axial direction, a constant spacing of 0.05 m is used. The fixed grid window moves downwards with the current injection node staying in a central position on the borehole axis. For all models, a borehole radius of 0.1 m and a mud resistivity of 1 Ω m are chosen.

3.2 Resistive layer

The resulting parameter curves are displayed in Figs 3–5. Each figure consist of four diagrams. On the left-hand side, the model geometry and the layer resistivities are shown. The borehole is presented as a grey bar on the left-hand side. The second graph shows the parameter curve ρ_a/ρ_m of the second difference configuration and the third graph is the curve of the resistivity ratio ρ_a/ρ_m of the combined lateral configuration. The graph on the rightmost side presents the logarithm of the quotient of the current ratios of the Laterolog-7. The layer boundaries of the model are marked by thin horizontal lines in all graphs.

The first example consists of a broad (2 m thick) homogeneous layer with a true resistivity of 50 Ω m embedded in a homogeneous environment of 10 Ω m (see Fig. 3).

The parameter curve ρ_a/ρ_m of the second difference configuration shows a small maximum 0.1 m above the upper layer boundary. A simple physical explanation can be given for the shift. The second difference of the potential corresponds to the current flowing horizontally into the formation. Directly above the resistive bed, a larger amount of current flows into the conductive formation. Close to the lower boundary, a slight minimum inside the resistive layer is visible.

The parameter curve ρ_a/ρ_m of the combined lateral configuration shows a broad maximum at the upper layer boundary with an extreme

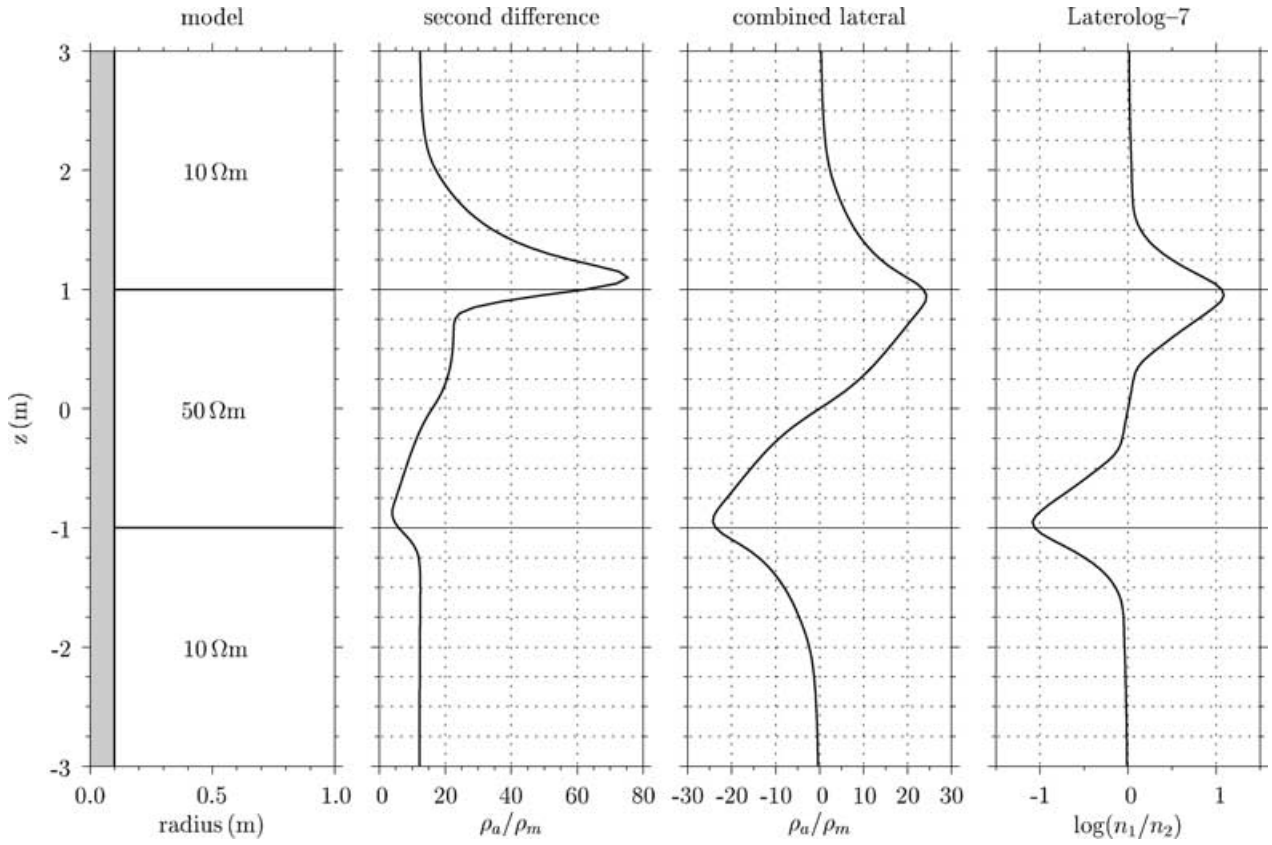

Figure 3. Curves of indication parameters for a homogeneous layer.

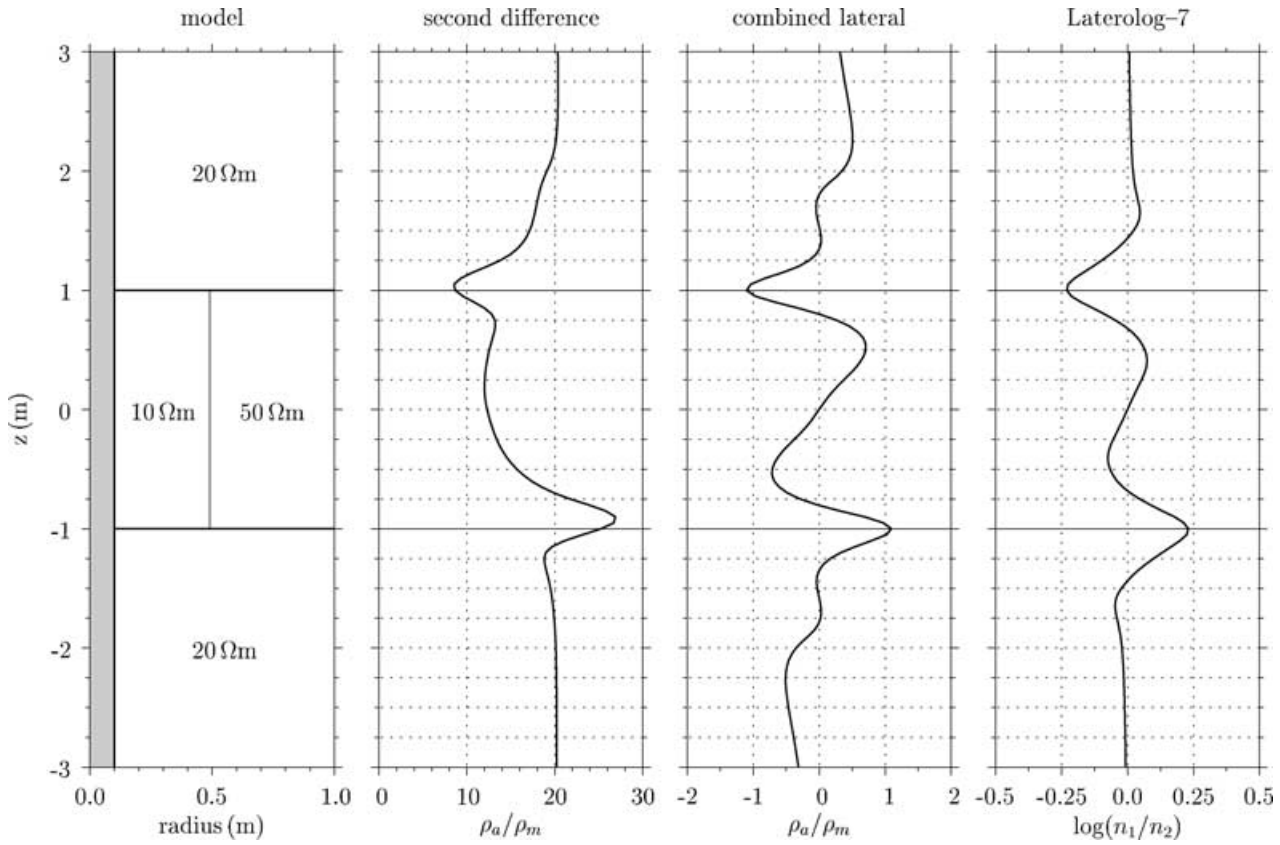

Figure 4. Curves of indication parameters for an invaded layer.

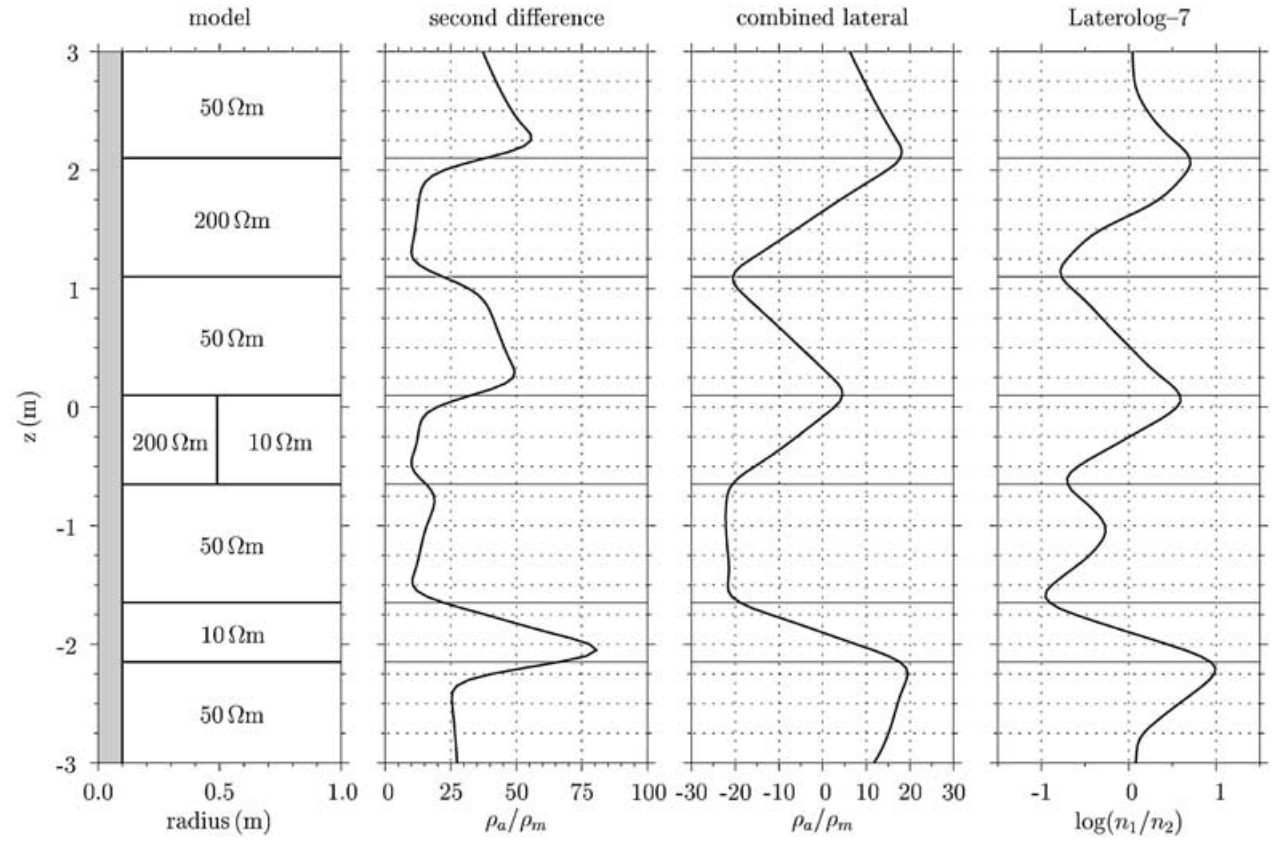

Figure 5. Curves of indication parameters for a sequence of seven layers.

value one gridpoint below the boundary. At the lower boundary ($z = -1$ m), an inverse structure is visible. The minimum is reached one gridpoint above the boundary.

The structure of the parameter curve resulting from Laterolog-7 is similar to that of the combined lateral configuration. The upper layer boundary is marked by a significant maximum (shifted one gridpoint to the resistive side) and the lower by a minimum (shifted one gridpoint to the resistive side too). In comparison with the combined lateral configuration, the shape of the Laterolog-7 curve better accentuates the layer boundaries.

3.3 Invaded layer

In the second example, a layer with invasion is embedded in a homogeneous formation. The model and the resulting curves are presented in Fig. 4. In contrast to the first example, there exists a vertical boundary in the embedded layer at a radius of 0.49 m. The inner part of this layer corresponds to the invasion zone. The model resistivities are 20 Ω m in the homogeneous formation, 10 Ω m in the invasion zone and 50 Ω m in the undisturbed formation.

The parameter curve of the second difference configuration shows two extreme values, a minimum at the upper and a maximum at the lower boundary. Both are shifted one or two grid points upwards. The structure is not really antisymmetric about the origin $z = 0$.

The other two curves, the combined lateral configuration and Laterolog-7, present antisymmetric structures with respect to the origin $z = 0$ m. In comparison with the first example, the curve shapes become more complicated. In both curves, two additional distinct extreme values at $z = 0.5$ and -0.5 m can be identified. In the case of the combined lateral configuration, the absolute values of these additional extreme values are comparable with those at the model boundaries. Using this curve, two additional horizontal layer boundaries will be detected at these depth points. In the case of the Laterolog-7, the absolute values of the two additional extreme values reach only one-third of those at the model boundaries, so they can be eliminated by a cut-off of absolute values.

3.4 Sequence of seven layers

In the two previous examples, the main features of the three curves are shown for a broad layer with or without invasion. In order to obtain more information concerning vertical resolution of the three configurations a sequence of seven layers of different resistivity and thickness is chosen next. Fig. 5 presents the model and the results. Layers 1, 3, 5 and 7 represent a homogeneous formation with a resistivity of 50 Ω m. The second layer is homogeneous with a resistivity of 200 Ω m and a thickness of 1 m. The fourth layer is invaded with an inner resistivity of 200 Ω m and a formation resistivity of 10 Ω m. The vertical boundary is located at $r = 0.49$ m and the thickness of the layer is 0.8 m. The sixth layer is conductive with a resistivity of 10 Ω m and a thickness of 0.4 m.

As in the two previous examples, the parameter curve of the second difference configuration indicates the upper boundary of the resistive bed and the lower boundary of the conductive bed by maximal values. The invaded layer is identified as a resistive layer with a maximum at the upper boundary. The opposite boundaries are only visible as a slight minimum. All extreme values are located slightly above the model boundaries.

The combined lateral configuration clearly indicates four of the six bed boundaries. A problem exists in the region between the lower boundary of the invaded layer and the upper boundary of the conductive layer. At the lower boundary of the invaded layer a minimum is reached, but no increase of the parameter ρ_a/ρ_m is visible until the upper boundary of the conductive layer is reached. The structure looks like a plateau. The configuration is not able to mark clearly the two adjacent transitions from resistive to conductive beds.

The current ratio curve of Laterolog-7 shows the best results. All model boundaries are indicated by a strong extreme value. The invaded layer is identified as a resistive layer. Also the two adjacent transitions from resistive to conductive beds where the combined lateral configuration was ineffective are clearly resolved. As seen in the preceding examples, the extreme values are shifted by approximately one grid distance to the resistive side for all transitions.

According to the results of these three simple synthetic examples, it can be noticed that the combined lateral device and the Laterolog-7 are able to identify both types of transitions (conductive–resistive and resistive–conductive), but the second difference configuration shows only a distinct structure at the transition from conductive to resistive layers if the tool moves downwards. It seems difficult to identify a transition from resistive to conductive beds with this special second difference tool.

3.5 Relation between the indication parameter and the resistivity contrast

Here, the *indication parameter* of all considered configurations is defined in such a way that a maximum occurs at the downward transition from a conductive to a resistive layer and a minimum at the downward transition from a resistive to a conductive layer. The sign of the extreme value clearly indicates the type of transition. In a further step, it is investigated whether the absolute value of the indication parameter is related to the resistivity contrast of the adjacent beds. A model consisting of two layers of infinite thickness is considered. As in the other examples, the mud resistivity and the borehole diameter are fixed. The extreme values of the indication parameter at the layer boundary are determined as a function of the resistivity contrast between the adjacent layers ρ_2/ρ_1. The resulting curves are displayed in Fig. 6 for three different ratios between the resistivity of the lower layer ρ_1 and the mud resistivity ρ_m.

The diagram of the second difference configuration in Fig. 6(a) shows continuously rising curves reaching different asymptotic values for the contrasts ρ_1/ρ_m. Since the three curves are crossing it does not seem possible to derive the resistivity contrast ρ_2/ρ_1 from the extreme value of the indication parameter without knowledge of the mud resistivity ρ_m.

In the case of the combined lateral configuration (Fig. 6b), the three curves approach a similar asymptotic value. The extreme value of the indication parameter becomes less sensitive to the resistivity ratio ρ_2/ρ_1 if the ratio ρ_1/ρ_m increases.

As shown in Fig. 6(c), the three curves of the Laterolog-7 configuration are close to each other for low-resistivity contrast ρ_2/ρ_1. The effect of the mud resistivity seems to be less important. A nearly linear behaviour can be assumed up to $\rho_2/\rho_1 = 100$. The slope becomes smaller for higher ratios, especially for the highest contrast $\rho_1/\rho_m = 100$.

Such diagrams can be built for any borehole radius and resistivity contrast. Investigations by Pusch *et al.* (1988) have shown that not only the resistivity contrast but also the layer thickness and the spacing of the Laterolog-7 affect the current ratios. Considering all of these effects, these diagrams can be used to estimate the resistivity contrast at the boundary. Using the logarithm of the quotient of the current ratios, Pusch *et al.* (1988) qualitatively classified the

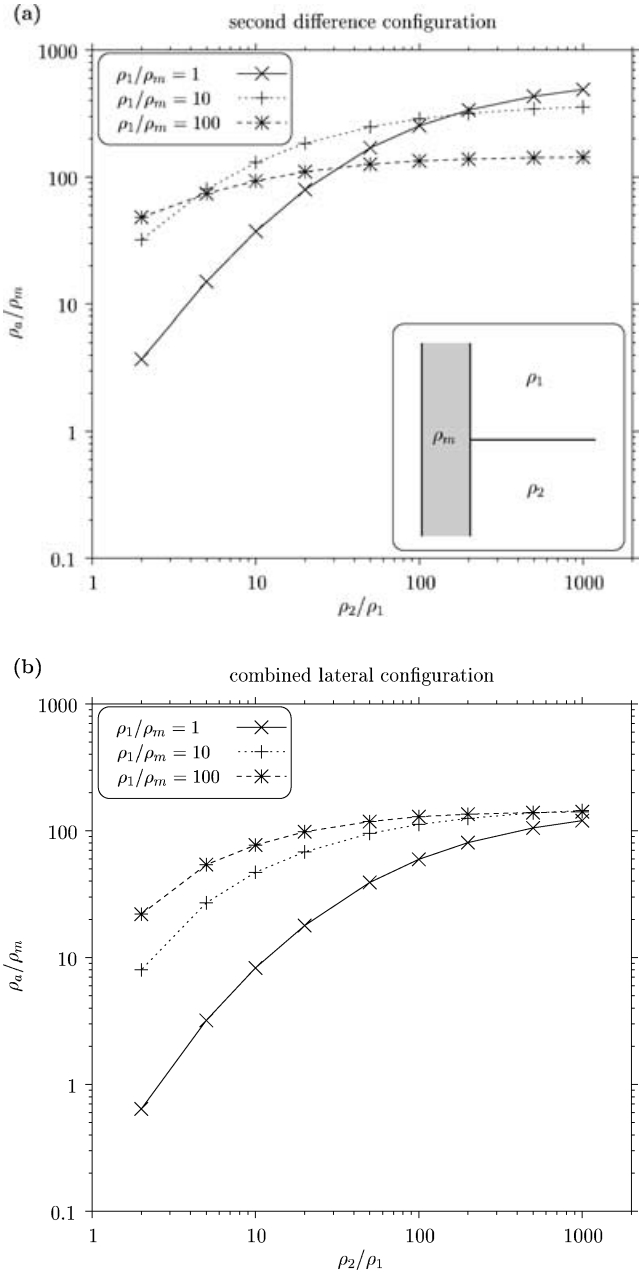

Figure 6. Relation between the resistivity ratio ρ_1/ρ_2 of two infinite layers and the indication parameter for three different resistivity ratios ρ_1/ρ_m. (a) Second difference configuration; (b) combined lateral configuration (c) Laterolog-7.

resistivity contrast. A moderate resistivity contrast is expected for absolute values larger than 0.5. Based on Fig. 6(c), these values correspond to a resistivity ratio of ρ_2/ρ_1 larger than 2. This classification is a helpful tool for fixing a threshold value for neglecting low-contrast boundaries.

4 TEST WITH MEASURED DATA

A test of the algorithm for layer identification was made using log data of a prototype nine-electrode tool that is shown in Fig. 2(a). In a first step the raw electrical data were filtered using a *Butterworth* filter of second order with a cut-off wavelength of 1 m. The filtered data from the tool are displayed together with the natural gamma

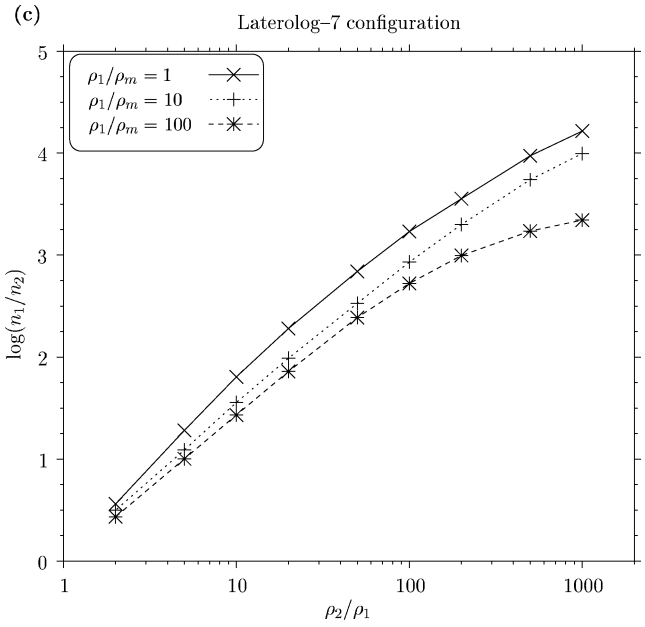

Figure 6. (*Continued.*)

log and the synthetic Laterolog-7 in Fig. 7. The lithological profile of the test well is presented on the left-hand side of the figure. The formation is a succession of layers of sandstone, shaly sandstone and shale of different thickness. The layer boundaries were determined using the gamma-ray log. The resistivity of the mud filtrate amounts to 1 Ω m at a depth of 42 m and decreases to 0.5 Ω m at 79 m. The potentials measured at electrodes M_1–M_8 are transformed into apparent resistivities. The resulting curves of potential configurations are close to each other with the smallest values belonging to the smallest spacing. It would be difficult to identify all layers using only these apparent resistivity data. The synthetic Laterolog-7 was calculated using the potential values at electrodes M_1, M_2, M_4 and M_5 (Weller 1986). The resulting apparent resistivity curve more clearly identifies the transition between layers of different resistivity.

The parameter curves for the detection of layer boundaries are presented in Fig. 8. It is investigated whether the layer boundaries that are marked in the lithological profile can be identified by the parameter curves based only on electrical data. First, a threshold value for each curve has to be fixed. Only extreme values that exceed a certain limit indicate layer boundaries. All other peaks are neglected. As proposed in the preceding section for a moderate contrast, ± 0.5 was selected as the threshold value for the Laterolog-7. This value corresponds to a layer resistivity contrast of 2, which is nearly independent of the resistivity contrast between formation and mud.

In the case of the combined lateral configuration, the resistivity contrast between formation and mud has a great influence on the parameter curve (see Fig. 6b). For low layer resistivity contrasts, the parameter curve increases with increasing resistivity contrast between formation and mud. For a layer resistivity contrast of 2 and a formation–mud contrast of 100 a parameter value ρ_a/ρ_m of 25 is determined in the synthetic example. Since the average resistivity contrast between formation and mud is greater than 100, a threshold value of abs $(\rho_a/\rho_m) = 40$ is chosen to resolve the same layer resistivity contrasts as with the Laterolog-7.

It is very difficult to chose a threshold in the case of the second difference configuration. For a layer resistivity contrast of 2

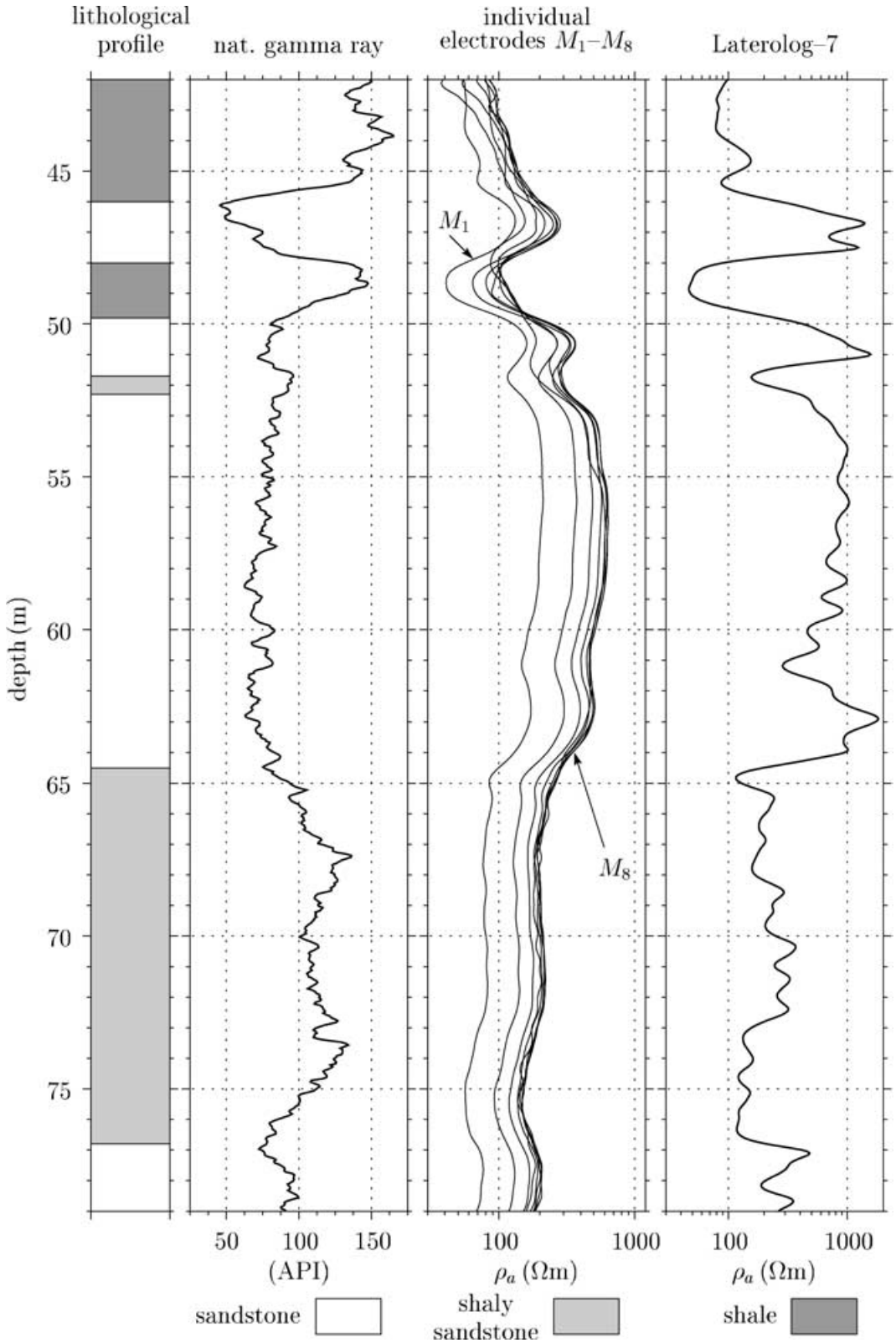

Figure 7. Lithological profile, natural gamma-ray data log, apparent resistivities measured by the eight individual electrodes and apparent resistivity of the synthetic Laterolog-7.

the parameter curve shows an ascending tendency with increasing resistivity contrast to the mud. To indicate the same boundaries as the other two configurations, a threshold value of $\rho_a/\rho_m = 200$ has proved to be appropriate. Since the transition from resistive to conductive layers is barely detected by the second difference configuration the threshold value is only valid for the maxima.

In the next step, the extreme values exceeding the thresholds are identified and marked in the figure as horizontal lines for each

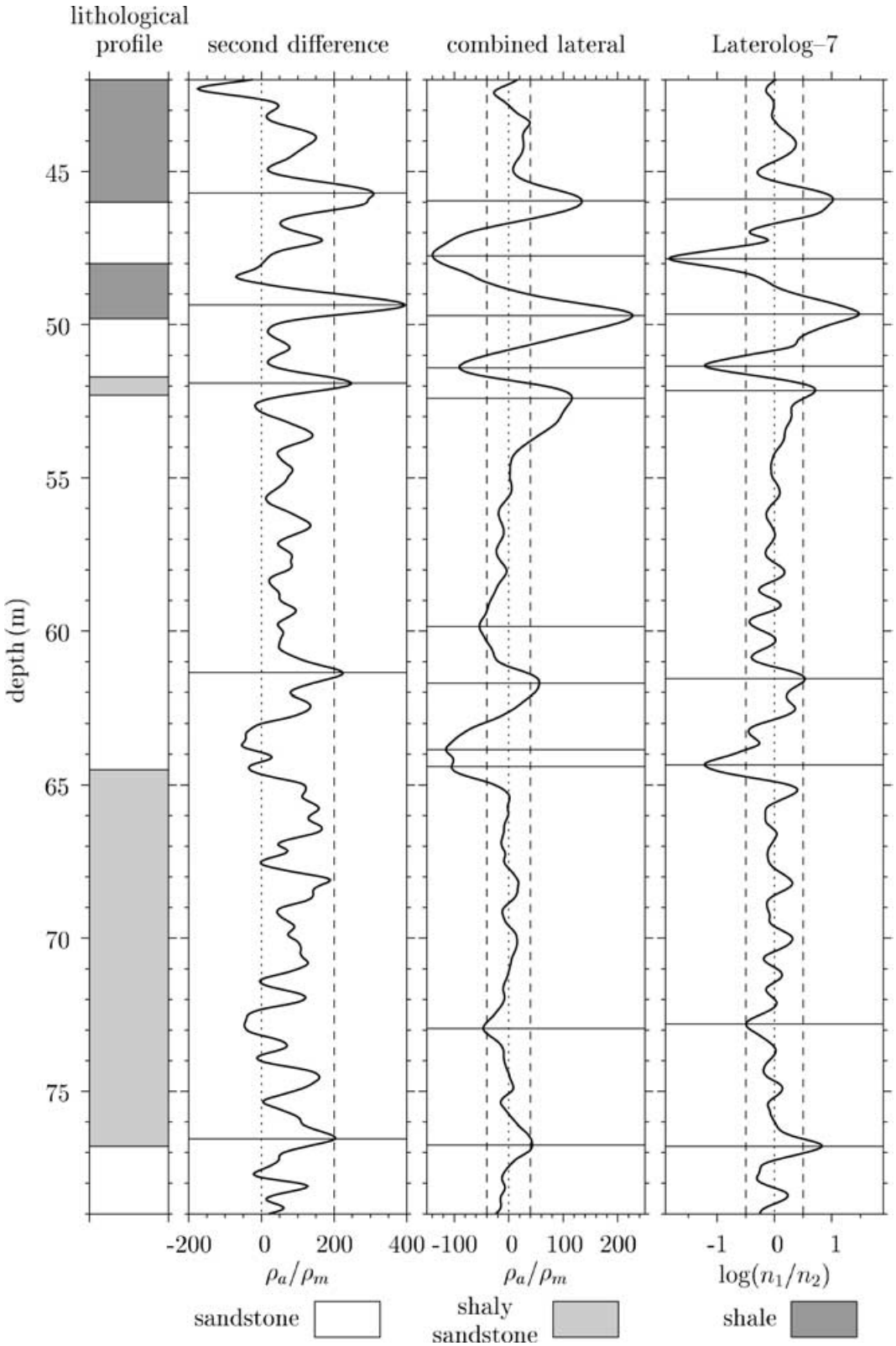

Figure 8. Lithological profile, indication parameter curves of second difference configuration, combined lateral configuration and Laterolog-7.

configuration. At a depth of 46 m, the lithological profile indicates a first boundary from shale to sandstone, which means a transition to a more resistive layer. All three curves show a corresponding maximum in the vicinity of this transition. As in the synthetic examples the maximum is slightly shifted upwards for the second difference configuration.

The next boundary at 48 m is identified by a minimum of both the combined lateral configuration and the Laterolog-7. Since this has

to be a transition from a resistive to a conductive layer no indication is expected from the second difference configuration. The next boundary between shale and sandstone (conductive–resistive) is located at 49.8 m. Similar to the first boundary all configurations show a significant maximum in the parameter curve. The upper boundary of a thin shaly sandstone layer at 51.7 m is clearly seen in the curves of the combined lateral configuration and the Laterolog-7. Its lower boundary, which forms the transition to a thick sandstone layer at 52.2 m, is indicated by a maximum in all three curves.

This sandstone layer is characterized by a low level of natural gamma-ray activity (<90 API) and resistivity values > 300 Ω m in the Laterolog-7 curve. From the varying resistivity values in both the normal logs and the Laterolog-7, it can be concluded that the sandstone layer is not homogeneous. Between 59.9 and 61.7 m the combined lateral configuration resolves a more conductive layer. Its lower boundary is confirmed by the two other configurations, too. A closer look at the Laterolog-7 curves shows a slight minimum that does not reach the threshold at the upper boundary of this intermediate layer. Since there is no clear indication in the gamma-ray log a change to a finer grain size or higher porosity can be assumed. The lower boundary of the sandstone layer at 64.4 m is marked by a double minimum for the lateral combined configuration and a single minimum for the Laterolog-7.

The transition to the more conductive shaly sandstone is also reflected by an increase of the gamma-ray activity. In the shaly sandstone bed, another resistivity decrease is observed in the Laterolog-7 curve (see Fig. 7) that results in an additional boundary at a depth of 72.8 m, which is indicated by both the combined lateral and Laterolog-7 parameter curve. Finally, the lower boundary of the shaly sandstone layer at 76.8 m is well indicated by maxima in all parameter curves. It marks the transition to another sandstone layer.

5 RESULTS AND CONCLUSIONS

The examples of synthetic models show that the investigated second difference tool is able to resolve a downward transition from conductive to resistive layers by a strong maximum in the curve of the ratio between apparent resistivity and mud resistivity. This maximum is shifted to the conductive side. For the measured data, all transitions of this type are detected by the second difference configuration. The downward transition from resistive to conductive beds is hardly visible in the curves, so this type of transition cannot be detected. The second difference configuration is very sensitive to data noise.

The combined lateral tool is a zero-potential configuration. It records non-vanishing potential differences only in inhomogeneous media. This property is used to identify layer boundaries. The configuration resolves both resistive to conductive and conductive to resistive transitions with the same amplitude but a different sign. The parameter curve indicates the position of the layer boundary by an extreme value and the type of transition by the sign. Some problems occur for invaded layers where additional extreme values come up, which indicate boundaries erroneously. Another problem occurs for sections where the distance between transitions of the same type becomes too small. Such structures cannot clearly be identified as two separate boundaries. For the measured data set, all boundaries that are known from the lithologic log are well detected. One boundary is reflected by a double minimum. This behaviour implies that some transitions cannot be described by a single jump in resistivity. The transition may be divided into several small jumps or the resistivity changes more or less continuously in a certain depth interval. More investigation is necessary to select reliable criteria for the threshold value. Since only first differences are used for calculating this parameter the sensitivity to data noise is smaller compared with the other two configurations.

For the Laterolog-7 device, the logarithm of the quotient of the current ratios has to be determined as the most sensitive parameter for detection of layer boundaries. The resulting curves look similar to that of the combined lateral tool. The major advantage is a better resolution of a sequence of layer boundaries within a short distance. Another advantage is the quantitative relation to the resistivity contrast between the adjacent layers. So it is easier to fix the threshold for neglecting small-amplitude peaks that are caused by noisy data. For the measured data set, the Laterolog-7 is able to detect all boundaries known from the lithologic log. Some additional layer boundaries are found at places where the resistivity curves also show a visible change.

Based on a 2-D FD code, our investigation was restricted to a vertical borehole and horizontal layering. Wang *et al.* (2000) calculated the dual Laterolog response for dipping layers using a 3-D finite-element algorithm. Their results show that the changes of apparent resistivity curves are negligible up to a dip angle of 30°. Only in the case of greater dip angles do the changes become significant. From these results it can be concluded that the parameter curves for detecting layer boundaries proposed in this paper can also be used in the case of slightly dipping layers (dip angle < 30°).

Our aim in more recent work is the further improvement of the inversion algorithm for multi-electrode resistivity data. Based on an investigation of the sensitivity distribution of different borehole electrode configurations we have shown the superior ability of the Laterolog-7 to resolve thin layers and to approximate the true resistivity (Furche & Weller 2002). In this paper, we have proved the ability of the Laterolog-7 and the combined lateral configuration to identify layer boundaries. An estimate of the layer resistivity and the positioning of the layer boundaries are important steps for an inversion procedure. The results of data inversion will be reported in a forthcoming paper.

ACKNOWLEDGMENTS

The work was carried out in co-operation with the firm Brunnen- und Bohrlochinspektion GmbH within the framework of a project that was supported by the Federal Ministry of Economics and Technology (BMWi). The prototype of the nine-electrode resistivity tool was manufactured by the firm LogIn Bohrlochmessgeräte GmbH, Gommern. We are very grateful to Max Meju and an anonymous reviewer for their useful comments and suggestions.

REFERENCES

Dey, A. & Morrison, H.F., 1979. Resistivity modeling for arbitrarily shaped three-dimensional structures, *Geophysics,* **36,** 753–780.

Fan, X., 1998. Modellierung und Inversion von gleichstromgeoelektrischen Bohrlochmessungen mit 2D- und 3D-Finite-Differenzen, *Dissertation,* Berlin, Techn. University.

Furche, M. & Weller, A., 2002. Sensitivity distributions of different borehole electrode configurations considering a model with a cylindrical coaxial boundary, *Geophys. J. Int.,* **149,** 338–348.

Hakvoort, R.G., Fabris, A., Frenkel, M.A., Koelman, J.M.V.A. & Loermans, A.M., 1998. Field measurements and inversion results of the high-definition laterolog log, *39th Ann. SPWLA meeting,* Society of Professional Well Log Analysts.

Lowry, T., Allen, M.B. & Shive, P.N., 1989. Singularity removal: a refinement of resistivity modelling techniques, *Geophysics,* **54,** 766–774.

Meijerink, J.A. & van der Vorst, H.A., 1977. An iterative solution method for linear systems of which the coefficient matrix is a symmetric *M*-matrix, *Math. Comp.,* **31,** 148–162.

Mezzatesta, A.G. & Eckard, M.H., 1995. Joint inversion combines galvanic and induction data to enhance accuracy of estimated formation parameters, *In Depth,* **1,** 32–40.

Mufti, I.R., 1976. Finite-difference resistivity modeling for arbitrarily shaped two-dimensional structures, *Geophysics,* **41,** 62–78.

Pusch, C., 1990. Untersuchungen zu fokussierenden Widerstandsmeßanordnungen in der Bohrlochmessung, *Freib. Forsch.-H., C,* **444,** 3–45.

Pusch, C., Schön, J. & Weller, A., 1988. Eine Multipotentialsonde-Prinzip und Perspektiven in der Bohrlochmessung, *Z. angew. Geol.,* **34,** 169–172.

Schön, J. & Weller, A., 1984. Calculation of synthetic resistivity curves by finite-difference method and approximate focusing filter operation, *Trans. 9th Int. Formation Evaluation Symp.,* paper 23, Societé poor l'Avancement de lïuterprétation des diagraphies-Section de la SPWLA.

Spitzer, K., 1995. A 3-D finite-difference algorithm for DC resistivity modelling using conjugate-gradient methods, *Geophys. J. Int.,* **123,** 903–914.

Vallinga, P.M., Harris, J.R. & Yuratich, M.A., 1991. A multi-electrode tool, allowing more flexibility in resistivity logging, *Trans. 14th Eur. Formation Evaluation Symp.,* paper E, Society of Professional Well Log Analysts.

Wang, H., Shen, L.C. & Zhang, G.J., 2000. Dual Laterog response in 3-D environments, *Petrophysics,* **41,** 234–241.

Weller, A., 1986. Berechnung geoelektrischer Potentialfelder mit dem Differenzenverfahren, *Freib. Forsch.-H., C,* **405,** 68–122.

Weller, A., Schön, J. & Rösler, R., 1984. Die Berechnung synthetischer Widerstands-Bohrlochmeßkurven nach der Methode der finiten Differenzen, *Neue Bergbautechnik,* **14,** 87–90.

Weller, A., Seichter, M. & Kampke, A., 1996. Induced-polarization modelling using complex electrical conductivities, *Geophys. J. Int.,* **127,** 387–398.

Whitman, W.W., Towle, G.H. & Kim, J.H., 1989. Inversion of normal and lateral well logs with borehole compensation, *Log Anal.,* **30,** 1–11.

Whitman, W.W., Schön, J., Towle, G. & Kim, J.H., 1990. An automatic inversion of normal resistivity logs, *Log Anal.,* **31,** 10–19.

Yuratich, M.A. & Meger, W.J., 1984. The application of finite difference methods to normal resistivity logs, *Trans. 25th SPWLA Annual Logging Symp.,* paper V, Society of Professional Well Log Analysts.

Zhang, Z. & Zhou, Z., 2002. Real-time quasi-2-D inversion of array resistivity logging data using neuronal network, *Geophysics,* **67,** 517–524.

Zhang, J., Mackie, R.L. & Madden, T.R., 1995. 3-D resistivity forward modeling and inversion using conjugate gradients, *Geophysics,* **60,** 1313–1325.

Zhang, Z., Frost E., Jr, Chunduru, R. & Mezzatesta, A., 2002. Petrophysically constrained inversion of resistivity logging data, *Petrophysics,* **43,** 82–91.